J Mater Sci (2009) 44:179–185
DOI 10.1007/s10853-008-3101-4

Synthesis and characterization of niobium-doped potassium tetragonal tungsten bronzes, $K_xNb_yW_{1-y}O_3$

Tapas Debnath · Subrata Chandra Roy · Claus H. Rüscher · Altaf Hussain

Received: 7 July 2008 / Accepted: 3 November 2008 / Published online: 27 November 2008

Abstract Needle-shaped crystals of sizes up to 5 μm × 5 μm × 40 μm of nominal composition $K_xNb_yW_{1-y}O_3$ were synthesized by solid state method at 800 °C using appropriate amount of WO_3, WO_2, Nb_2O_5, and K_2WO_4. The samples were characterized with XRD, SEM, microprobe analysis, optical spectroscopy, and Raman spectroscopy. The XRD patterns of the samples show single phase of tetragonal tungsten bronze (TTB) type (P4/mbm, No. 127) up to $y = 0.07$. Structure refinements reveal an increase in cell parameter with increasing nominal niobium content within the TTB phase. The elemental compositions of the crystals determined by electron microprobe analysis also show an increase in Nb content with increasing y. With increasing Nb content the reflectivity minimum in the near infrared spectral range shifts towards lower wavenumber indicating the effect of decreasing carrier concentration. Pyrochlore type phase ($KNbWO_6$) is obtained as a second phase when nominal composition $y > 0.07$.

Introduction

Tungsten bronzes, M_xWO_3, are non-stoichiometric phases of ternary metal oxides where M is typically an electropositive metal atom and $0.0 \leq x \leq 1.0$. Tungsten bronzes have four different structure types; perovskite-type tungsten bronzes (PTB) [1, 2], tetragonal tungsten bronzes (TTB) [3], hexagonal tungsten bronze (HTB) [4], and intergrowth tungsten bronzes (ITB) [5] depending on the size and amount of M (for review see Ref. [6]). These bronzes have been intensively studied because of interesting technological applications such as electronic devices, humidity and gas sensor, secondary batteries, and ion-sensitive electrodes [7–9] (see also Ref. [10] and references therein). The electrical, superconducting, and optical properties, e.g., for the HTB system (M_xWO_3, M = K, Cs, Rb) have been reported [11–13], which can be modified depending on x within the stability field $0.2 \leq x \leq 0.33$. The x-dependent superconductivity has been reinvestigated more recently [14–16]. Moreover, it has also been reported that Nb could be substituted in these types of systems leading to modified optical and electrical properties [17]. Similar effect has been reported for the perovskite cubic system with nominal composition $Na_xNb_yW_{1-y}O_3$ ($x = 0.8$ and $y = 0.0$–0.4) [18]. Therefore, the aim of this study was to investigate the effect of substitution of W by Nb in non-stoichiometric tetragonal potassium tungsten bronze (K-TTB).

The structure of tetragonal potassium tungsten bronzes (K-TTB, K_xWO_3) consists of a framework of corner sharing WO_6 octahedra, with tunnels of trigonal, square, and pentagonal shape running along the short crystallographic c axis (Fig. 1). The pentagonal and to some extent the tetragonal tunnels are occupied by K atoms. The compositional range, x, reported for K-TTB is 0.42–0.57 [19]. The chemical formula of alkali metal tungsten bronzes can be written also as $M_x^+(W_x^{5+}W_{1-x}^{6+})O_3$ showing the degree of reduction of the bronzes depending on the value of x with the formation of nominal W^{5+} state. This assumption is supported by Yan et al. [20] and Gu et al [21] who investigated the TTB and

T. Debnath (✉) · C. H. Rüscher
Institut für Mineralogie und Zentrum für Festkörperchemie und neue Materialien (ZFM), Leibniz Universität Hannover, Callinstraße 3, 30167 Hannover, Germany
e-mail: tapas.debnath@mineralogie.uni-hannover.de

S. C. Roy · A. Hussain
Department of Chemistry, University of Dhaka, Dhaka 1000, Bangladesh

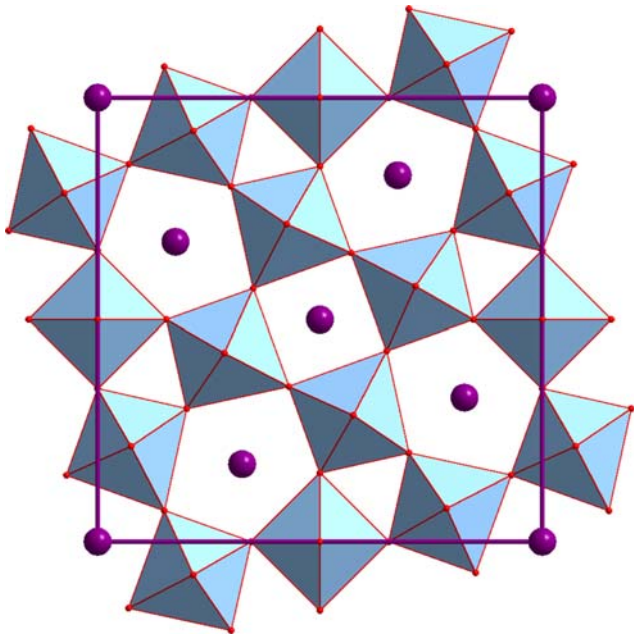

Fig. 1 Crystal structure of tetragonal tungsten bronze (TTB), projected along *c*-axis

HTB phases of K_xWO_3 by XPS spectroscopy and reported only the presence of W^{5+} and W^{6+} states of W. The formation of W^{4+} state has been discussed recently for $(NH_4)_{0.33-x}WO_{3-y}$ type compounds [22, 23].

It might be suggested that W^{5+} can be replaced by other pentavalent ions, e.g., Nb^{5+}, according to $M_x(Nb_yW_{1-y})O_3$ and the question was how far this could lead to a counterdoping effect in K-TTB bronzes. When $y = x$, the phase becomes fully oxidized, which has been called "bronzoids" [24]. Synthesis and characterization of fully niobium-substituted tetragonal potassium tungsten bronzoids has been reported earlier [25]. Here we report for the first time, the partially niobium substituted tetragonal potassium tungsten bronzes.

Experimental

Samples of various nominal compositions $K_xNb_yW_{1-y}O_3$ ($x = 0.55$ and $y = 0.0$–0.15) were prepared by reaction in evacuated sealed silica glass tubes at 800 °C according to Eq. 1.

$$x/2\ K_2WO_4 + (1 - x - y/2)WO_3 + (x - y)/2\ WO_2 + y/2\ Nb_2O_5 = K_xNb_yW_{1-y}O_3 \quad (1)$$

$$K_2CO_3 + WO_3 = K_2WO_4 + CO_2 \quad (2)$$

$$K_2WO_4 + WO_3 + Nb_2O_5 = 2KNbWO_6 \quad (3)$$

The materials initially used were WO_3 (99.998%), WO_2 (99.9%), Nb_2O_5 (99.9985%), and K_2WO_4. All the reactants except K_2WO_4 were from Alfa Aesar. K_2WO_4 was prepared by heating equimolar mixtures (according to Eq. 2) of K_2CO_3 (99.95%, Alfa Aesar) and WO_3 (99.998%) in air at 600 °C for 4 days. $KNbWO_6$ (pyrochlore type phase) was prepared by heating equimolar mixtures (according to Eq. 3) of K_2WO_4, WO_3 and Nb_2O_5 in air in an open silica glass tube at 800 °C for 3 days. The purity of all reactants were checked by taking X-ray powder pattern and found as single phase. Appropriate amount of reactants were mechanically mixed in an agate mortar and transferred into clean, dry silica glass tubes (6–8 mm inner diameter and about 100 mm in length). The tubes were evacuated (0.13 Pa) at room temperature for about two hours, sealed, and then put directly in a pre-heated Muffle Furnace at 800 °C. Under these conditions the samples were held for 7 days. Finally, the reaction tubes were cooled to room temperature by taking out of the furnace.

The products were characterized by X-ray powder diffraction method using a Guinier-Hägg focusing camera (CuKα_1 radiation) and a Bruker D8 diffractometer (transmission geometry, CuKα radiation). Structure refinements were performed using the Rietveld software Diffrac Plus TOPAS (Bruker AXS, Karlsruhe, Germany). For the calculation of the reflex profiles, fundamental parameters were used on the basis of instrumental parameters calculated out of a silicon standard measurement. As an additional general parameter the zero point of the center was varied, and a polarization parameter was fixed. For the structure calculation, the TTB structure type model (space group no. 127) was used. The absolute value of lattice parameters was determined from the X-ray powder photographs taken by Guinier-Hägg focusing camera using Si as internal standard ($a = 5.430879$ Å, CuKα_1 radiation). For the calculations, the photographs were scanned using an automatic film scanner [26] and evaluated using computer programs SCANPI and PIRUM [27].

The scanning electron microscopy (SEM) images of samples were taken in JEOL-6060. The elemental compositions were analyzed with a "CAMECA SX-100" electron microprobe. For microprobe analysis, polycrystalline samples were glued to plane sample holder (ordinary glass) and mechanically abraded and finally polished (0.2 μm diamond paste) and coated with a carbon layer. All data were obtained using 15-kV acceleration potential, a static (fixed) beam, K_α emission from potassium, L_α emission from Nb, and M_α emission from tungsten. The standard Nb on Nb, W on W, and K on orthoclase (composition: O = 46.11%, Na = 0.33%, Al = 9.09%, Si = 30.56%, K = 13.03%, Fe = 0.88%) were used for calibration. The samples were analyzed with a focused beam, 15 nA beam current and counting times of 3 s for each element. A beam diameter of about 2 μm was used.

The VIS-NIR reflectivity of powder samples were measured in the range of 8500–20000 cm^{-1} against KBr powder as a reference by using Bruker IFS88 FTIR spectrometer equipped with a device for integrating the reflectivity scattered over a larger angle (Spectra Tech. INC).

IR absorption spectra were measured in KBr-method where 1 mg of the finely ground sample was dispersed into 199 mg KBr and pressed into pellet (13 mm diameter). Measurements were done in the range of 220 cm^{-1}–4000 cm^{-1} (Bruker IFS66v FTIR spectrometer equipped with standard DTGS detector).

The MIR micro-reflectivity (650–5000 cm^{-1}) of the polished samples was measured using a FTIR spectrometer (Bruker IFS88) with an attached microscope. Raman measurements were done on polished samples using a confocal Raman microscope (CRM 200, frequency doubled Nd:YAG laser with maximal power of 20-mW). All spectra were obtained in backscattering geometry using a microscope device that allows the incident light to be focused on the sample as a spot of about 2 μm in diameter.

Results and discussion

The X-ray diffraction patterns of the samples having nominal composition $y \leq 0.07$ show pure single phase and could be indexed as TTB type phase (Fig. 2a, b). The samples with nominal niobium content $y > 0.07$ show TTB phase and also an additional phase, which could be indexed as a cubic pyrochlore type phase (Fig. 2c, d). For the TTB phase Rietveld refinements reveal a very good agreement between the experimental and theoretical pattern using space group P4/mbm supporting earlier results for TTB phases of composition K_xWO_3 [19]. Data of our investigation show that Nb-substituted forms are isostructural with the TTB phase. As a typical example, the detail of the structural parameters obtained for the sample $y = 0.07$ by Rietveld method, are given in Tables 1 and 2.

A distorted cubic pyrochlore type phase (ICDD 21–1003) [28] along with TTB found as second phase in the XRD pattern of nominal compositions $y \geq 0.1$ was included in the refinement using space group Fd-3 m (Fig. 2c, d). A quantitative Rietveld refinement estimated that the weight fraction of pyrochlore type phase for $y = 0.10$ and $y = 0.15$ samples is about 6% and 10%, respectively. The lattice parameters of the corresponding samples are given in Table 3. There is a slight increase in lattice parameters with increasing Nb content up to $y = 0.07$. For $y = 0.10$ and 0.15 the lattice parameters do not increase further (Table 3), indicating the stability limit has been reached in TTB phase. The values obtained from the diffractometer data are systematically less by about 1 pm than that of the Guinier data.

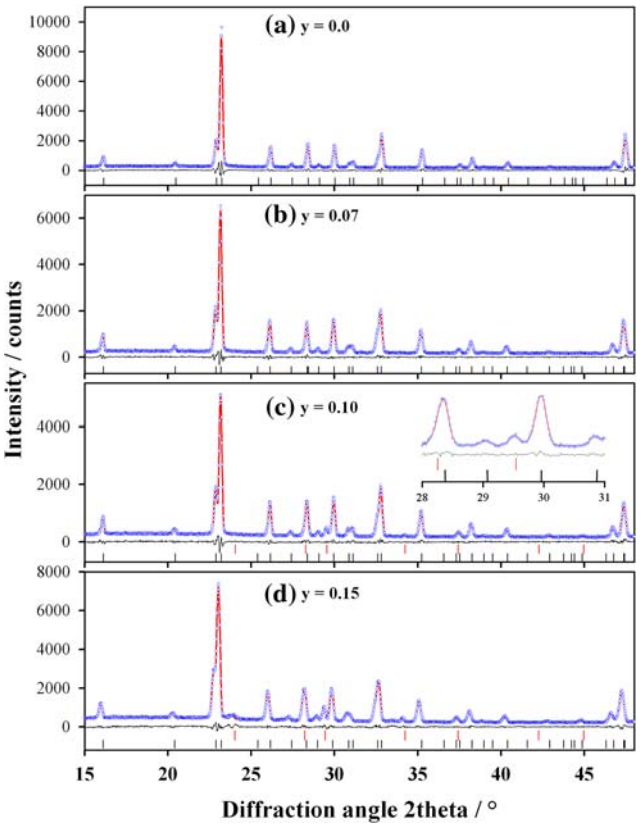

Fig. 2 Observed X-ray diffraction pattern (dotted) and calculated pattern (solid line) using the Rietveld method for samples (**a**) $y = 0$; (**b**) $y = 0.07$; (**c**) $y = 0.10$, and (**d**) $y = 0.15$. The respective difference curve and indexed peak positions (bars) are also shown. The black and red "bars" show the calculated peak positions of TTB and pyrochlore type phase, respectively. Inset ((**c**), $y = 0.1$) shows the 222 diffraction line at $2\theta = 29.55°$ for pyrochlore type phase. Rietveld refinements were done in whole measured range ($2\theta = 10$–$100°$), but, for the sake of clarity the diffraction patterns were shown in the range of $2\theta = 15$–$50°$

Such deviations are generally accepted when cell parameters are determined from these two methods. The evidence of Nb substitution in K-TTB is clearly shown in the following when the results of microprobe analysis are taken into account. The increase in relative amount of pyrochlore type phase and the decrease in TTB phase contribution with increasing nominal composition y showing that the stability limit for Nb substitution (in TTB) has been reached for $y = 0.07$ under the present synthesis conditions.

Scanning electron microscopy (SEM) images of the samples are shown in Fig. 3. Crystallites with rectangular morphology are clearly visible in the images. The maximum size of the rectangular crystals is up to 5 μm × 5 μm × 40 μm. The SEM images of the sample with nominal $y \geq 0.10$ shows some additional octahedral shaped crystals up to 10 μm size edges. It is observed that the octahedral shaped crystals are mainly pyrochlore type phase.

Table 1 Crystallographic data for $K_{0.47}Nb_{0.07}W_{0.93}O_3$. Rp, Rwp, and GOF refer to the Rietveld criteria of fit as defined in the manual of the "TOPAS Diffrac Plus" program

Formula	$K_{0.47}Nb_{0.07}W_{0.93}O_3$
Temperature (K)	298
Space group	P4/mbm
Z	10
a (Å)	12.2826(3)
b (Å)	12.2826(3)
c (Å)	3.8332(1)
V (Å^3)	578.275(29)
ρ-cal (g/cm^3)	6.8680(4)
2θ range (°)	10–100
Step size (°2θ)	0.02
Wavelength (Å)	Cu$K\alpha$ radiation
μ (1/cm) (cryst. Linear abs. coefficient)	924.12(5)
Rp	6.15%
Rwp	7.81%
GOF	1.26

The results of microprobe analysis are given in Table 3. The experimental Nb content of the TTB phase fits well with the nominal composition of the samples up to $y = 0.07$. The samples with nominal composition $y > 0.07$ show Nb content is about 0.06(2) for the needle-shaped crystals, which supports that the maximum amount of doped Nb is about 0.07(2) in TTB phase. The pyrochore type crystals (octahedral shape crystals) show Nb content as 0.49(2). The potassium contents range in all cases between 0.46 and 0.48, which is systematically lower than the nominal value (0.55) implying a systematic loss during synthesis. The potassium content (TTB phase, $y = 0.0$) calculated from the cell parameters [3, 19] is between 0.45 and 0.50, which is also a bit less than the nominal composition, $x = 0.55$. An increase in lattice parameter values with increasing amount of substitution of Nb^{5+} or Ta^{5+} has been observed in cubic perovskite tungsten bronzes, $Na_xNb_yW_{1-y}O_3$ and $Na_xTa_xW_{1-y}O_3$ [18, 29, 30]. This trend is also observed in $K_xNb_yW_{1-y}O_3$, too. The composition found for the pyrochlore type phase (ICDD 21–1003) from the microprobe analysis is $K_{0.47(3)}Nb_{0.49(2)}W_{0.51(2)}O_3$. Taking into account the standard deviation of the microprobe analysis, the composition may be written as $K_{0.50}Nb_{0.50}W_{0.50}O_3$ ($\equiv KNbWO_6$). The formation of pyrochlore type phase in this field is not unexpected and has been reported during the synthesis of bronzoid type phase, too [25, 28, 31].

The VIS-NIR reflectivity of the samples was measured in the spectral range between 8500 and 20000 cm^{-1}. The pure TTB (i.e. $y = 0$) sample shows a pronounced

Table 2 Atomic coordinates and displacement parameter of $K_{0.47}Nb_{0.07}W_{0.93}O_3$

Atom	Site	x	y	z	Occ.	Biso
K	2a	0.00000	0.00000	0.00000	0.207(19)	2.78(28)
K	4g	0.17225(64)	0.67225(64)	0.00000	0.982(25)	2.78(28)
W	2c	0.00000	0.50000	0.50000	0.907(63)	1.458(37)
W	8j	0.07540(18)	0.20793(17)	0.50000	0.891(65)	1.458(37)
Nb	2c	0.00000	0.50000	0.50000	0.0931	1.458(37)
Nb	8j	0.07540(18)	0.20793(17)	0.50000	0.1093	1.458(37)
O	2d	0.00000	0.50000	0.00000	1	2.04(21)
O	8i	0.0740(15)	0.2103(15)	0.00000	1	2.04(21)
O	4h	0.2899(14)	0.7899(14)	0.50000	1	2.04(21)
O	8j	−0.0020(10)	0.3485(17)	0.50000	1	2.04(21)
O	8j	0.1457(14)	0.0754(21)	0.50000	1	2.04(21)

Table 3 Cell parameters and microprobe analysis data of $K_xNb_yW_{1-y}O_3$

Composition x		Composition y		Crystal structure	Cell parameter (Diffractometer)		Cell parameter (Guinier)	
Nominal	Microprobe	Nominal	Microprobe	(Rietveld)	a/pm	c/pm	a/pm	c/pm
0.55	0.46(1)	0.00	0.0	TTB	1226.47(3)	382.71(1)	1227.8(1)	382.88(8)
0.55	0.46(2)	0.05	0.03(1)	TTB	1227.98(4)	383.18(1)	1229.5(2)	383.54(2)
0.55	0.47(1)	0.07	0.07(2)	TTB	1228.26(3)	383.32(1)	1229.6(1)	383.63(8)
0.55	0.48(1)	0.10	0.06(2)	TTB + (about 94%),	1228.23(4)	383.32(2)	–	–
	0.47(3)		0.49(2)	Pyrochlore (about 6%)	1048.83(4)	–	–	–
0.55	0.46(3)	0.15	0.06(2)	TTB + (about 90%),	1228.10(5)	383.36(4)	–	–
	0.46(3)		0.48(2)	Pyrochlore (about 10%)	1048.79(6)	–	–	–

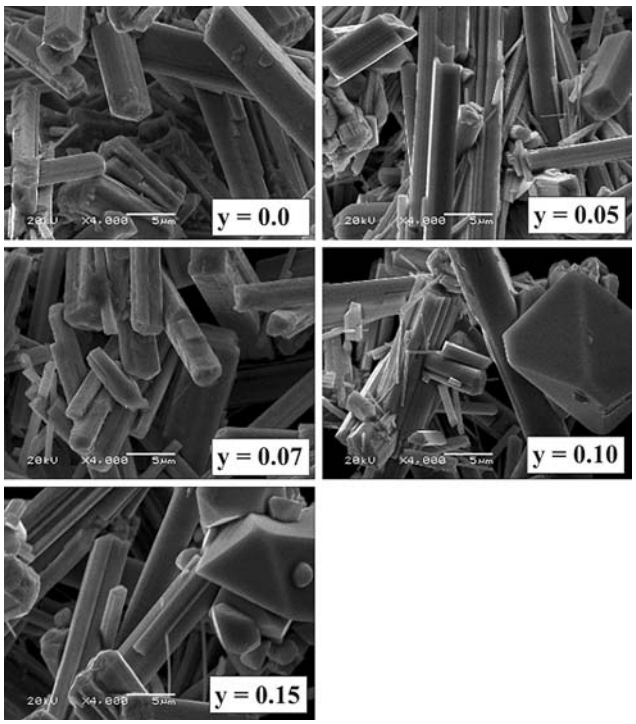

Fig. 3 Scanning electron micrograph of $K_{0.55}Nb_yW_{1-y}O_3$ samples showing typical TTB phase (needle-type crystals) in all compositions but pyrochlore type phase (octahedral shaped crystals) can be seen only when gross composition, $y \geq 0.1$

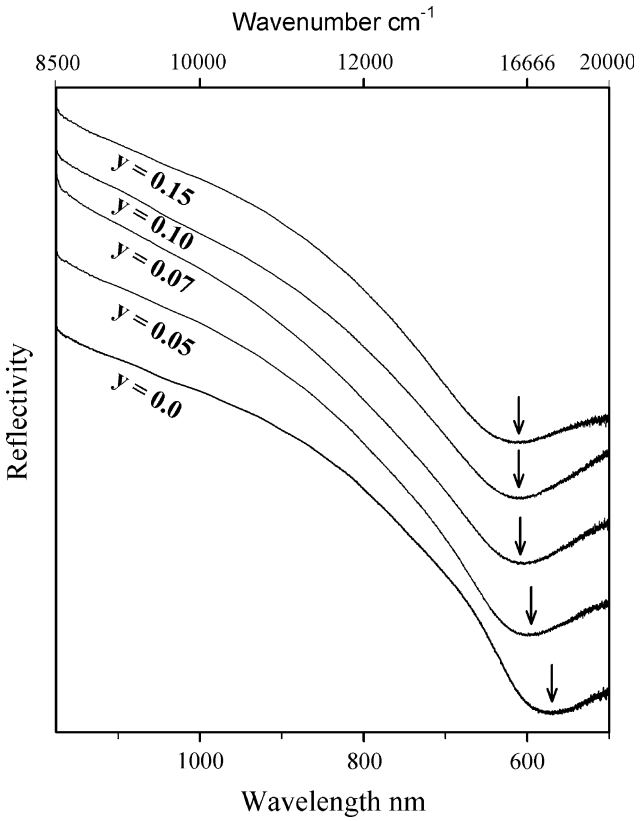

Fig. 4 VIS-NIR reflectivity spectra of powder samples showing the shift of minima toward the low wavenumber (as marked with arrow) with increasing Nb content. The spectra are shifted vertically for the sake of clarity

minimum at about 17500 cm^{-1} together with a sharp increase in reflectivity toward lower wavenumber (Fig. 4). For $y = 0.05$ and 0.07 sample the minima position is shifted to about 16700 and 16400 cm^{-1}, respectively. The position of the minima for the $y = 0$ sample is in very good agreement with the minima reported earlier [13] for K-TTB single crystals of composition $K_{0.5}WO_3$ for the electrical field polarized parallel to the c axis (E//c). Having the potassium content fixed as authenticated by microprobe for the series here the shift of the reflectivity minima toward lower wavenumber can entirely be related to the effect of Nb substitution which thus decreases the effective amount of W^{5+}. Similar effect has been reported by Hussain et al. [17] for $Rb_xNb_yW_{1-y}O_3$ HTB system. In a simple free carrier picture for a rigid lattice, the position of the reflectivity minimum related to the plasma edge of the carriers is proportional to the square root of the relative charge carrier concentration (Eq. 4).

$$\omega_P = \sqrt{\frac{Ne^2}{m^*\varepsilon_\infty}} \tag{4}$$

(ω_P = plasma frequency, N = concentration of carriers, e = charge of electron, m* = effective electron mass, and ε_∞ = effective high-frequency dielectric constant.)

The effect of Nb doping may be written formally as $K_x(Nb_y^{5+}W_{x-y}^{5+}W_{1-x}^{6+})O_3$. Considering the chemical formula for sample with nominal composition $y = 0.07$ ($\equiv K_{0.5}Nb_{0.07}^{5+}W_{0.43}^{5+}W_{0.5}^{6+}O_3$), the concentration of effective charge carriers would be 0.43 (i.e., $x - y$). Thus, for a counterdoping effect of $y = 0.07$ a shift of the minima by a factor of $(0.43/0.5)^{1/2}$ can be expected for $K_{0.5}Nb_{0.07}W_{0.93}0_3$, i.e., to about 16230 cm^{-1} which is close to the value observed experimentally. For the $y \geq 0.1$ samples, no further shift is observed indicating that a maximum of counterdoping effect has been reached for y less than 0.1.

Figure 5 shows the IR spectra of nominal $K_{0.55}Nb_yW_{1-y}O_3$ series, where the samples $0.0 \leq y \leq 0.07$ show the characteristic increase, typical for metallic samples, e.g. ReO_3 [32], which could be explained as proportional to (1 − R), where R is the Drude reflectivity. Similar results have been reported for Nb-doped HTB system [17]. The appearance of broad peak for nominal $y \geq 0.10$ is due to the systematic development of second phase (pyrocholore type, $KNbWO_6$) (see XRD results, Table 3). For direct comparison, the IR absorption spectrum of pure $KNbWO_6$ phase is included in Fig. 5. Calculated IR absorption spectrum using the as-measured IR absorption spectra of 90% pure TTB ($y = 0.07$) + 10% pure $KNbWO_6$ generates almost similar feature as for the IR absorption

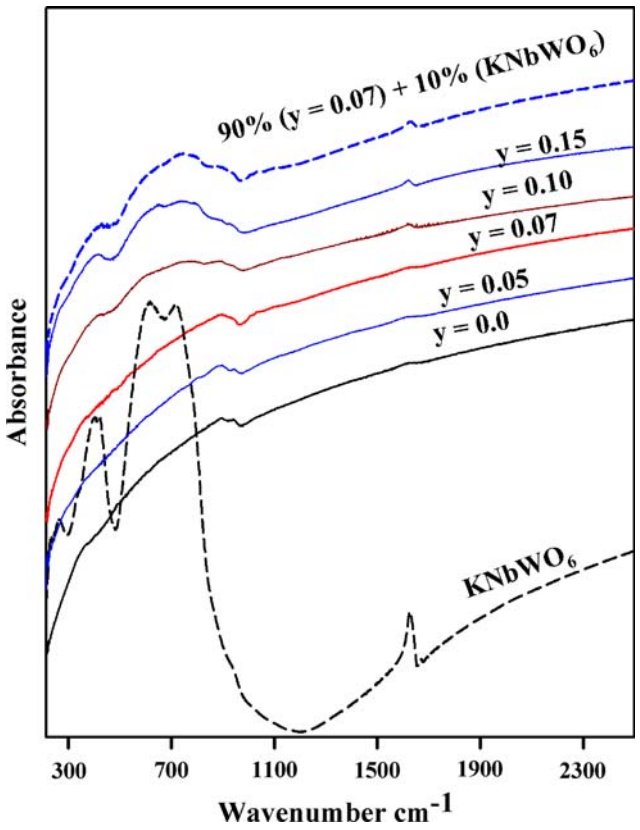

Fig. 5 IR spectra (KBr-method) of nominal $K_{0.55}Nb_yW_{1-y}O_3$ series. The spectra are shifted vertically for the sake of clarity. The broad peaks below 1000 cm^{-1} for samples $y \geq 0.1$ are due to the presence of pyrochlore type phase. The IR absorption spectrum of pure $KNbWO_6$ is also included (as denoted). Calculated spectrum (as denoted), in addition with as-measured spectra of 90% ($y = 0.07$) + 10% $KNbWO_6$, shows similar IR absorption feature of nominal $y = 0.15$ sample

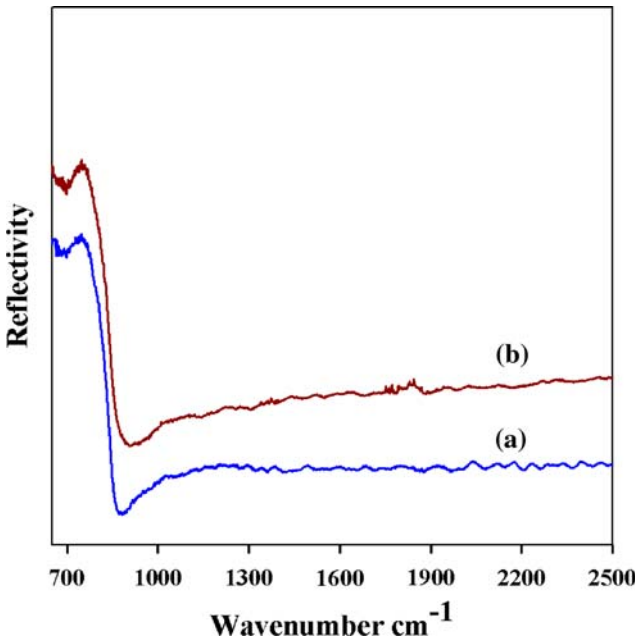

Fig. 6 Micro-reflectivity spectra of "white crystallites" (pyrochlore type phase) observed within samples (a) $y = 0.1$ and (b) $y = 0.15$. The spectra are shifted vertically for the sake of clarity

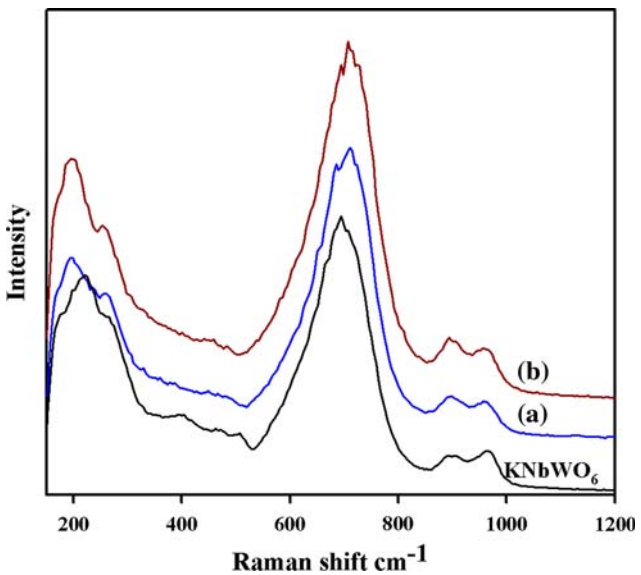

Fig. 7 Raman spectra of "white crystallites" (pyrochlore type phase) of samples with nominal (a) $y = 0.1$ and (b) $y = 0.15$. Raman spectrum of $KNbWO_6$ is also included (as denoted). The spectra are shifted vertically for the sake of clarity

spectrum of nominal $y = 0.15$ (Fig. 5), which support the XRD results where a mixture of about 90% TTB and 10% $KNbWO_6$ has been estimated (Table 3). The IR absorption peaks of pure $KNbWO_6$ centered at about 650 cm^{-1} is due to the M–O (M = Nb or W) stretching mode, which can be compared with the IR absorption spectrum of $NaNbWO_6$ [33]. The absorption peaks below 450 cm^{-1} is likely to be due to the bending mode of M–O.

Optical micrographs of polished samples show the presence of additional "white crystallites" for nominal $y \geq 0.1$ which is due to the formation of pyrochlore type phase as explained before (by XRD, Microprobe, IR absorption spectra). For independent proof, the micro-reflectivity of "white crystallites" measured on polished samples for nominal composition $y = 0.10$ and 0.15, are shown in Fig. 6. The MIR reflectivity spectra of "white crystallites" are identical for both samples and shows a phonon with maximum at about 745 cm^{-1}, which can be assigned to the M–O stretching mode.

The Raman spectra of "white crystallites", at temperature 298 K, (Fig. 7) are also characteristic for $KNbWO_6$. For direct comparison, the Raman spectrum of pure $KNbWO_6$ phase is included in Fig. 7. Moreover, the main peaks in Raman spectrum of pyrochlore type phase can be described considering the Raman study of $NaNbWO_6$, $Na_{1.2}Nb_{1.2}W_{0.8}O_6$, and $KNbW_2O_9$ from the literatures

[33–35]. The Raman peak above 900 cm^{-1} can be assigned to the stretching mode of terminal –M = O (M = Nb/W) bonds. The highest intense peak at about 700 cm^{-1} and the peaks below 450 cm^{-1} can be assigned to the stretching and bending modes of MO_6 octahedra, respectively.

Conclusion

Tetragonal potassium tungsten bronzes, K_xWO_3, and its niobium-substituted forms, $K_xNb_yW_{1-y}O_3$, have been prepared by conventional solid state method at temperature 800 °C. The X-ray powder patterns reveal that the pure tetragonal tungsten bronze type phase can be prepared up to nominal composition $y = 0.07$. For $y \geq 0.10$ distorted pyrochlore type phase of composition $K_{0.5}Nb_{0.5}W_{0.5}O_3$ was observed. This showed that in the applied preparation way and with the applied experimental parameters, pure niobium-doped TTB phase forms only if $y < 0.1$. The increase of Nb content in the samples (i.e., increase in y) could be authenticated by electron microprobe analysis, by the systematic increase in the lattice parameters and by the shift of the plasma edge of the carriers reduced by Nb substitution.

Acknowledgement AH is grateful to the Alexander von Humboldt Stiftung, Germany, and University Grants Commission, Bangladesh for financial support. TD thanks the "Land Niedersachsen", Germany for support with the "Lichtenberg Stipendium" for his Ph.D. research fellowship. Finally, the authors are thankful to two anonymous referees for their helpful comments.

References

1. Hägg G (1935) Z Phys Chem B 29:192
2. Magnéli A (1950) Nova Acta Regiae Soc Sci Upsaliensis 14:4
3. Magnéli A (1949) Arkiv for Kemi 1:213
4. Magnali A (1953) Acta Chem Scand 7:315
5. Hussain A, Kihlborg L (1976) Acta Crystallogr A32:551
6. Labbe Ph (1992) Key Eng Mater 68:293
7. Tsuyumoto I, Kudo T (1996) Mat Res Bull 31:17
8. Granqvist CG (2000) Sol Energ Mater Sol Cells 60:201
9. Gabel J, Vonau W, Shuk P, Guth U (2004) Solid State Ionics 169:75
10. Mann M, Shter GE, Reisner GM, Grader GS (2007) J Mater Sci 42:1010. doi:10.1007/s10853-006-1384-x
11. Skokan MR, Moulton WG, Morris RC (1979) Phys Rev B 20:3670
12. Sato M, Grier BH, Shirane G, Fujishita H (1982) Phys Rev B 25:501
13. Hussain A, Gruehn R, Rüscher CH (1997) J Alloys Compd 246:51
14. Brusetti R, Haen P, Marcus J (2002) Phys Rev B 65:144528
15. Brusetti R, Bordet P, Marcus J (2003) J Solid State Chem 172:148
16. Leitus G, Cohen H, Reich S (2002) Physica C 371:321
17. Hussain A, Ul-Monir A, Murshed MM, Rüscher CH (2002) Z Anorg Allg Chem 628:416
18. Debnath T, Rüscher CH, Gesing TM, Koepke J, Hussain A (2008) J Solid State Chem 181:783
19. Hussain A (1978) Chem Commun Univ Stockholm 2:1
20. Yang X, Li C, Mo M, Zhan J, Yu W, Yan Y, Qian Y (2003) J Cryst Growth 249:594
21. Gu Z, Ma Y, Zhai T, Gao B, Yang W, Yao J (2006) Chem Eur J 12:7717
22. Szilágyi IM, Hange F, Madarász J, Pokol G (2006) Eur J Inorg Chem 17:3413
23. Szilágyi IM, Madarász J, Pokol G, Király P, Tárkányi G, Saukko S, Mizsei J, Tóth AL, Szabó A, Varga-Josepovits K (2008) Chem Matter 20:4116
24. Magnéli A (1989) In: 12th European Crystallographic meeting, Moscow
25. Deschanvres A, Frey M, Raveau B, Thomazea Jc (1968) Bull De La Societe Chim De France:3519
26. Johansson KE, Palm T, Werner PE (1980) J Phys E: Sci Instrum 13:1289
27. Werner PE (1970) Arkiv for Kemi 31:513
28. Raveau B, Thomazea Jc (1968) Comptes Rendus Hebd Des Seances De L Acad Des Sci Serie C 266:540
29. Miyamoto Y, Kume S, Doumerc JP, Hagenmuller P (1983) Mat Res Bull 18:1463
30. Dubson MA, Holcomb DF (1985) Phys Rev B 32:1955
31. Darriet B, Rat M, Galy J (1970) Comptes Rendus Hebd Des Seances De L Acad Des Sci Serie C 271:1324
32. Feinleib J, Scouler WJ, Ferretti A (1968) Phys Rev B 165:765
33. Kuhn A, Bashir H, Dos Santos AL, Acosta JL, García-Alvarado F (2004) J Solid State Chem 177:2366
34. Sanjuán ML, Kuhn A, Azcondo MT, García-Alvarado F (2008) Eur J Inorg Chem 2008:49
35. Maczka M, Hanuza J, Majchrowski (2001) J Raman Spectrosc 32:929